Title

Surface-Wave Coupling and Antenna Properties in Two Dimensions

Journal

IEEE Transactions on Antennas and Propagation, 65(10)

ISSN

0018-926X

Authors

Wang, Chao
Li, En
Sievenpiper, Daniel F

Publication Date

2017

DOI

10.1109/tap.2017.2738030

Peer reviewed

Surface-Wave Coupling and Antenna Properties in Two Dimensions

Chao Wang, *Student Member, IEEE*, En Li, *Member, IEEE*, and Daniel F. Sievenpiper, *Fellow, IEEE*

***Abstract*— Antennas are characterized by their gain and effective aperture area, and the coupling between two antennas in 3-D free space is governed by the Friis transmission equation. In this paper, we derive the properties of antennas in 2-D space, and the equivalent coupling equation. This is useful for evaluating surface-wave coupling between antennas that share the same ground plane or substrate. We propose a quantity which is the effective width for surface-wave coupling, and derive its value for an isotropic surface-wave radiator in two dimensions. We also determine the surface-wave directivity for dipole-like modes, which is relevant to many small planar antennas. The total coupling between two coplanar antennas is a combination of surface waves and space waves, and these two components are distinguished in simulations by calculating antenna coupling as a function of distance. Several simple examples are illustrated including patch and monopole antennas on various substrates. Quantifying the effective surface wave width can serve as a useful tool for optimizing the coupling between coplanar antennas.**

***Index Terms*— Effective aperture, effective width, gain, mutual coupling, surface waves, transmission equation.**

I. Introduction

MUTUAL coupling often occurs between antennas that share the same substrate or ground [1]–[3], and it plays an important role in many applications such as arrays, multi-in multi-out systems, or other colocated communication systems that share the same ground plane. Mutual coupling may increase the signal correlation among antennas and reduce the efficiency of multiantenna systems [4]–[7]. The coupling between antennas can be attributed to three components: 1) near-field coupling, in which the fields decay with distance as ρ^{-2} or ρ^{-3}; 2) free-space coupling, which has ρ^{-1} dependence; and 3) surface-wave coupling where the fields decay as $\rho^{-1/2}$ [8]. In order to design antennas to have low mutual coupling, it is useful to distinguish between the different kinds of mutual coupling and to have a method to quantify their effects.

Near-field coupling occurs when one antenna is in the reactive near-field zone of another antenna, which extends to a radius of roughly $\lambda/2\pi$. This kind of coupling dominates when antennas are closely spaced [9], but is insignificant at greater distances due to the rapid decay of the near-field components. Free-space wave coupling is due to the standard antenna radiation in the horizontal direction, propagating parallel to the substrate. This kind of coupling can be efficiently reduced only if the antenna radiation in horizontal directions is suppressed, such as by designing the antenna to have low gain toward the horizon. Surface-wave coupling is due to surface waves which are guided by the substrate and the ground plane [10]. This kind of coupling dominates at longer distances, or when other coupling components have already been minimized. There have been several attempts to reduce mutual coupling, especially surface-wave coupling between antenna elements. For example defected ground structures have been implemented by etching slots of different shapes in the ground plane [11]–[14] and using electromagnetic bandgap structures to reduce the surface waves [15]–[17]. Other approaches to reduce the surface-wave coupling include high-impedance surfaces [18], [19] or soft surfaces [20], [21]. However, the free-space coupling and surface-wave coupling mechanisms and their contributions are not clearly distinguished in previous papers.

In this paper, we introduce the effective width of an antenna which characterizes how strongly it couples to surface waves, and calculate the effective width of an isotropic surface-wave radiator. We then determine the directivity of a surface-wave radiator with a dipole-like distribution, which is different from its directivity for free-space waves. We then use these results to determine the 2-D equivalent to the Friis transmission equation, which characterizes the surface-wave coupling component between two antennas. Finally, we provide simulations of several simple examples and evaluate them in terms of effective width and effective aperture. It is expected that the approach presented here will be useful for designing antennas with low mutual coupling because it will enable the designer to identify the relative strength of the different coupling components in order to optimize the design. For example, this approach can help to illustrate whether additional coupling reduction can be obtained by further reducing surface-wave effects, or to design the maximum allowable substrate thickness or permittivity for a given antenna configuration.

Manuscript received September 23, 2016; revised April 22, 2017; accepted August 6, 2017. Date of publication August 11, 2017; date of current version October 5, 2017. This work was supported in part by the National Natural Science Foundation of China under Grant 61671123 and Grant 61001027, in part by AFOSR Contract FA9550-16-1-0093, and in part by the China Scholarship Council. *(Corresponding author: Chao Wang.)*

C. Wang is with the School of Electronic Engineering, University of Electronic Science and Technology, Chengdu 611731, China, and also with the University of California, San Diego, La Jolla, CA 92093 USA (e-mail: chaowang-alvin@outlook.com).

E. Li is with the School of Electronic Engineering, University of Electronic Science and Technology, Chengdu 611731, China (e-mail: lien@uestc.edu.cn)

D. F. Sievenpiper is with the University of California at San Diego, La Jolla, CA 92130 USA (e-mail: dsievenpiper@eng.ucsd.edu).

Color versions of one or more of the figures in this paper are available online at http://ieeexplore.ieee.org.

Digital Object Identifier 10.1109/TAP.2017.2738030

II. 2-D-Surface-Wave Transmission Equation

A. Antenna Effective Aperture From Blackbody Radiation

Our first goal is to calculate the 2-D effective width of an antenna for transmitting or receiving surface waves. This quantity $W_{\text{eff}} = G_2 W_i$ is the product of the effective width W_i of

an ideal 2-D isotropic radiator, and a 2-D gain component G_2. In this paper, the subscript 2 is used to distinguish this term from the 3-D directivity associated with free-space waves. The term W_{eff} is analogous to the effective aperture in three dimensions. Thus, it would seem straightforward to simply follow the derivation of the effective aperture for an isotropic radiator, but with reduced dimensionality. Unfortunately, nearly all texts on this subject base the derivation on calculating the effective aperture of an infinitesimal dipole, and dividing by its directivity. Fortunately, an alternative method exists based on the power radiated and received by an ideal blackbody, and this approach is amenable to derivation with reduced dimensionality. The 3-D derivation is briefly summarized here to illustrate that it produces the intended result, and then repeated for the 2-D case.

We begin by outlining the Rayleigh–Jeans law for the spectral brightness of a blackbody radiator [22]. In a 3-D cubical cavity of length a, the allowable modes are defined by

$$n_x^2 + n_y^2 + n_z^2 = \left(\frac{2a}{\lambda}\right)^2. \tag{1}$$

Note that this is the standard starting point to calculate density of states in three dimensions, and is not related to the final size or shape of the antenna or radiating structure. The mode frequencies are

$$f = \frac{c}{\lambda} = \frac{cr}{2a} \tag{2}$$

where

$$r^2 = n_x^2 + n_y^2 + n_z^2. \tag{3}$$

The modes between f and $f + df$ are

$$N(f)df = \frac{4\pi r^2 dr}{8} \times 2 \tag{4}$$

where the factor of 2 is due to the two possible polarizations, and the factor of 1/8 is because we only need to consider positive indices for n, so we only integrate over 1/8 of the sphere in n-space.

Each mode has energy kT, so the spectral energy density assuming a cavity volume of a^3 is

$$u_f(T)df = \frac{N(f)df}{a^3} kT. \tag{5}$$

And

$$u_f(T) = \frac{8\pi a^3}{a^3}\frac{f^2}{c^3} kT = 8\pi kT \frac{f^2}{c^3}. \tag{6}$$

Because the radiation travels at velocity c, the spectral energy density is related to the spectral brightness B_3 as

$$u = \frac{1}{c}\int_{4\pi} B_3 d\Omega = \frac{4\pi}{c} B_3 \tag{7}$$

which has units of W/(sr m^3 Hz).

Thus

$$\frac{4\pi}{c} B_3 = u_f(T) = 8\pi kT \frac{f^2}{c^3}. \tag{8}$$

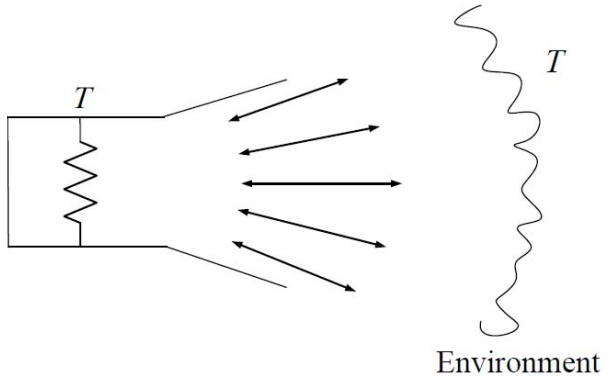

Fig. 1. Blackbody thermal equilibrium model.

And

$$B_3 = \frac{2kTf^2}{c^2} = \frac{2kT}{\lambda^2} \tag{9}$$

which is the Rayleigh–Jeans law [23], [24].

Now assume an isotropic antenna matched with a resistor at temperature T, which is in thermal equilibrium with its environment. It will radiate energy kT from the resistor, and it will receive an equal amount of energy from the environment, shown in Fig. 1. Using the spectral brightness calculated above, we can integrate over 4π steradians to determine the effective aperture A_e of an isotropic radiator. Because half of the power is radiated into one polarization, we divide B_3 by 2 to determine the effective aperture of an isotropic antenna for a single polarization

$$\frac{1}{2}\int B_3 d\Omega = \frac{1}{2}\int \frac{2kT}{\lambda^2} d\Omega = A_e 4\pi \frac{kT}{\lambda^2} = kT. \tag{10}$$

And

$$A_e = \frac{\lambda^2}{4\pi}. \tag{11}$$

This is consistent with the effective aperture calculated using other methods. The maximum effective aperture A_{eff} of any antenna is related to its gain G_3 by

$$A_{\text{eff}} = A_e \cdot G_3 = \frac{\lambda^2}{4\pi} G_3. \tag{12}$$

This density of states-based approach is also amenable to two dimensions, such as for surface-wave problems. We now apply this approach to determine the effective width of an isotropic radiator in two dimensions. This is also the effective width of an infinite line source in 3-D space.

B. Calculate the Effective Width for Surface Waves

In two dimensions, a square cavity has modes defined by

$$n_x^2 + n_y^2 = \left(\frac{2a}{\lambda}\right)^2 \tag{13}$$

and allowable frequencies

$$f = \frac{cr}{2a} \tag{14}$$

where

$$r^2 = n_x^2 + n_y^2. \tag{15}$$

The modes between f and $f+df$ are

$$N(f)df = \frac{2\pi r dr}{4} \times 2 \tag{16}$$

where we have integrated over 1/4 of the circle in n-space, and have included two polarizations.

The 2-D spectral energy density is

$$u_f(T)df = \frac{N(f)df}{a^2}kT. \tag{17}$$

And

$$u_f(T) = \frac{4\pi a^2}{a^2}\frac{f}{c^2}kT = 4\pi\frac{f}{c^2}kT. \tag{18}$$

The 2-D spectral brightness is

$$u = \frac{1}{c}\int_{2\pi} B_2 d\theta = \frac{2\pi}{c}B_2 \tag{19}$$

with units of W/(rad m^2 Hz).

Thus

$$\frac{2\pi}{c}B_2 = u_f(T) = 4\pi\frac{f}{c^2}kT. \tag{20}$$

And

$$B_2 = 2kT\frac{f}{c} = \frac{2kT}{\lambda}. \tag{21}$$

For an isotropic surface-wave radiator and one polarization, we multiply by the effective width W_i, and integrate over 2π to obtain the total radiated power, which is equal to kT

$$\frac{1}{2}\int B_2 d\theta = \frac{1}{2}\int \frac{2kT}{\lambda}d\theta = W_i 2\pi\frac{kT}{\lambda} = kT. \tag{22}$$

Thus, the effective width for an isotropic surface-wave radiator is found to be

$$W_i = \frac{\lambda}{2\pi}. \tag{23}$$

C. Calculate the Maximum Directivity and Maximum Effective Width of Antenna

As we know, the directivity of classic dipole antenna is 1.5 in free space

$$D_3 = \frac{4\pi}{\int_0^{2\pi}\int_0^{\pi}\sin^2\theta\sin\theta d\theta d\varphi} = 1.5. \tag{24}$$

For the 2-D case, we follow the 3-D case but only integrate over the azimuth. The surface-wave directivity of a dipole mode, that is, parallel to the surface is 2

$$D_2 = \frac{2\pi}{\int_0^{2\pi}\sin^2\varphi d\varphi} = 2. \tag{25}$$

For a vertical monopole antenna, the surface-wave directivity is $D_2 = 1$. Note that this is because the vertical null does not appear in the plane of the surface, so the antenna is isotropic with respect to surface waves.

In general, the maximum effective width W_{eff} of any antenna is related to its gain G_2 by

$$W_{\text{eff}} = W_i \cdot G_2 = \frac{\lambda}{2\pi}G_2. \tag{26}$$

Thus, when (26) is multiplied by the linear power density of the incident wave (in W/m), it leads to the maximum surface-wave power that can be delivered to the load. This assumes that there are no conductive or dielectric losses, the antenna is matched to the load, and the polarization of the impinging wave matches that of the antenna. For a transmitting antenna, this also assumes that all of the power couples into surface waves. Losses, polarization mismatch, and surface-wave coupling efficiency can be combined into a single-efficiency term, and gain is related to directivity D_2 and efficiency ζ_2 in the same way as in 3-D

$$G_2 = \zeta_2 D_2. \tag{27}$$

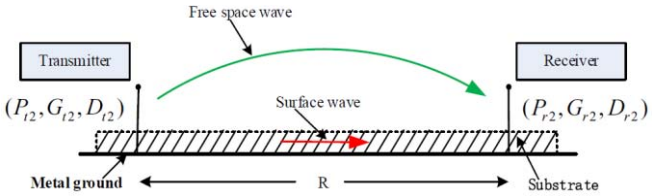

Fig. 2. Geometrical orientation of transmitting and receiving antennas for the transmission equation.

D. Calculate the 2-D-Surface-Wave Transmission Equation

The 2-D surface-wave transmission equation for mutual coupling between antennas relies on the transmitted and received power of the two array antennas placed in a distance. Referring to Fig. 2, let us assume that the transmitter is initially isotropic. If the input power at the terminals of the transmitting antenna is P_{t2}, then its maximum transmitted power density can be written as

$$S_{t2} = \frac{P_{t2}\zeta_{t2}D_{t2}}{2\pi R} = \frac{P_{t2}G_{t2}}{2\pi R} \tag{28}$$

where G_{t2} is the gain and D_{t2} is the directivity in the direction of the maximum of the surface wave. The maximum effective width W_{eff} of the receiving antenna is related to its efficiency ζ_{r2} and directivity D_{r2} by

$$W_{\text{eff}} = W_i \cdot \zeta_{r2}D_{r2} = \frac{\lambda}{2\pi}G_{r2}. \tag{29}$$

So the power P_{r2} collected by the receiving antenna can be written, using (28) and (29), as

$$P_{r2} = W_{\text{eff}}S_{t2} = G_{r2}\frac{\lambda}{2\pi}S_{t2} = G_{r2}\frac{\lambda}{2\pi}\frac{P_{t2}G_{t2}}{2\pi R} \tag{30}$$

or the ratio of the received to the input power as

$$\frac{P_{r2}}{P_{t2}} = \frac{G_{t2}G_{r2}}{4\pi^2}\frac{\lambda}{R}. \tag{31}$$

For impedance-matched and polarization-matched antennas aligned for maximum directional radiation and reception, (31) is the 2-D surface-wave transmission equation, and it relates the power P_{r2} (delivered to the receiver load) to the input power of the transmitting antenna P_{t2} in the same way as the Friis equation governs 3-D transmission. The term $\lambda/4\pi^2$R is the surface loss factor, and it takes into account the losses due to the spreading of the energy in two dimensions.

The total transmission including free-space wave coupling, surface-wave coupling, and mutual phase coupling between

the two antennas but neglecting near-field effects is

$$\frac{P_r}{P_t} = G_{t3}G_{r3}\left(\frac{\lambda}{4\pi R}\right)^2 + G_{t2}G_{r2}\frac{\lambda}{4\pi^2 R} + 2G_3G_2\frac{\lambda}{4\pi R}\sqrt{\frac{\lambda}{4\pi^2 R}}\cos\theta_R. \quad (32)$$

The first term is the standard Friis equation, the second term is the additional coupling due to surface-wave effects, and the third one is the mutual phase difference and resulting cross term in (32). The θ_R is the coupled phase difference between free space and surface wave, it can be obtained by

$$\theta_R = (k_{\mathrm{TM}} - k_0)\cdot R \quad (33)$$

where k_{TM} is the wavenumber of surface wave and k_0 is the wavenumber of free-space wave.

Consider a dielectric slab with permittivity ε_d and thickness h residing on a ground plane. For this configuration, we can have the equation is given by [25]

$$\frac{\varepsilon_d k_0^2 - k_{\mathrm{TM}}^2}{\varepsilon_d}\cdot h = \frac{\sqrt{k_{\mathrm{TM}}^2 - k_0^2}}{\varepsilon_0}. \quad (34)$$

From (34), we can see that if the thickness of the slab is very small, the wavenumber k_{TM} is almost equal to the wavenumber k_0. Thus, the total transmission equation is approximated by

$$\frac{P_r}{P_t} = G_{t3}G_{r3}\left(\frac{\lambda}{4\pi R}\right)^2 + G_{t2}G_{r2}\frac{\lambda}{4\pi^2 R} + 2G_3G_2\frac{\lambda}{4\pi R}\sqrt{\frac{\lambda}{4\pi^2 R}}. \quad (35)$$

By simulating the transmission between two identical antennas at various distances, we can determine the values of G_2 and G_3 separately, because they become fitting parameters in (35).

III. Comparison of Theoretical and Simulated Mutual Coupling

In this section, we will compare the mutual coupling theoretical results with numerical experiments using various lossless substrates. As described above, there are three kinds of mutual coupling between antennas, the near-field coupling, the free-space wave coupling, and the surface-wave coupling. Note that we are assuming lossless substrates, and we are focusing on the relative strength of the free space and surface-wave components. If the substrate is sufficiently loss, or the antennas are very close together, it is possible that the near-field term can be dominant [26], [27]. We will compare the results for the mutual coupling between a pair of rectangular patch antennas and a pair of monopole antennas. For all of the simulation results presented in this paper, the rectangular microstrip patch and monopole antennas are designed to operate at a frequency of 3 GHz ($\lambda = 100$ mm), with the same substrate and parameters shown in Figs. 3, 5, and 7. Ansys HFSS was used for the simulations, and the exterior surfaces of the simulation volume were all radiation boundaries.

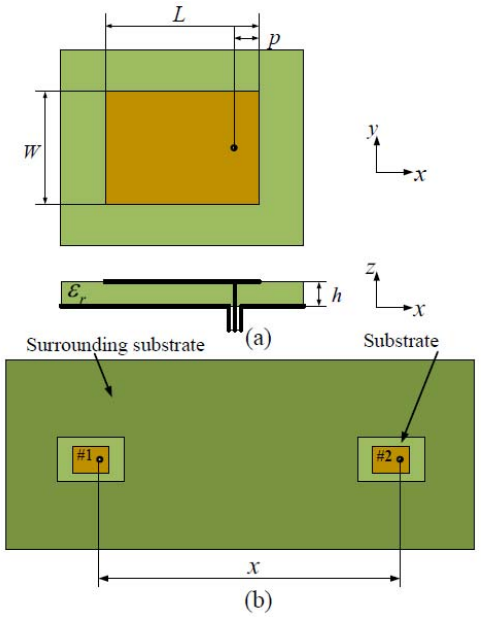

Fig. 3. (a) Top and view of classical microstrip antenna. (b) Coordinate system for coupled antennas.

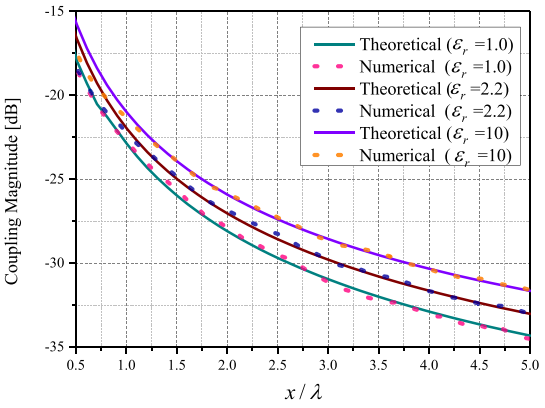

Fig. 4. Coupling comparison for the theoretical results and simulation results between microstrip antennas.

A. Rectangular Microstrip Patch Antenna

The geometry used in the calculation of the mutual coupling between two identical rectangular patch antennas is shown in Fig. 3(a). To exclude the influence of the substrate losses on the coupling, we only investigated antennas on lossless substrates. The substrate thickness is $h = 1.5$ mm and it has a relative dielectric constant ε_r of 5. Note that a small space is left around the patch with dielectric constant of 5, so that the same antenna design can be kept for surrounding substrates with different dielectric constants without having to retune the antenna design for each case. The patch length is $L = 21.3$ mm and the width is $W = 28.87$ mm. The patch is fed by a coaxial line, whose location is determined by matching conditions, and is set to $p = 3.2$ mm. In the computational models, we assume that the ground plane is infinite.

We evaluate the coupling between a pair of identical microstrip antennas which are printed on a lossless surrounding substrate with three different dielectric constants (1, 2.2, and 10). The dielectric constant below the patch was kept

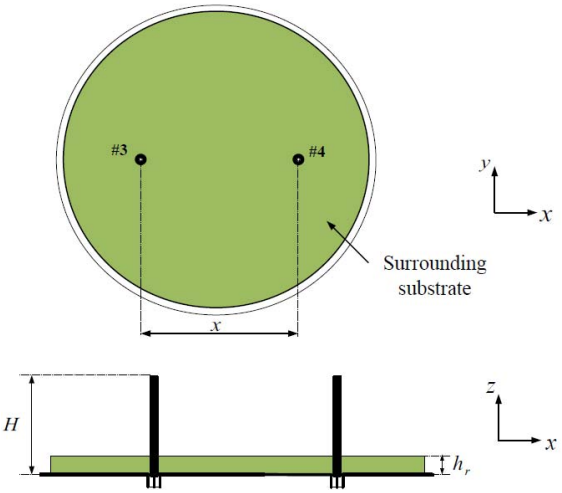

Fig. 5. Top and view of coupled monopole antennas.

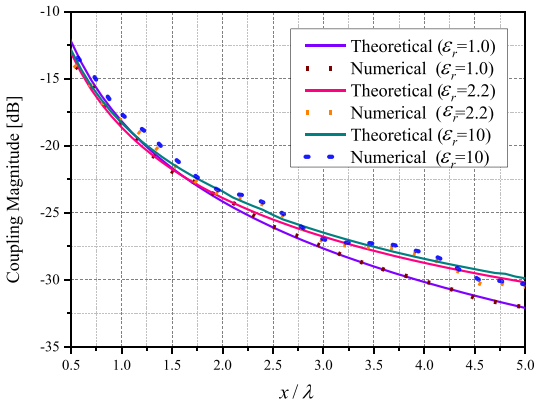

Fig. 6. Coupling comparison for the theoretical results and simulation results between monopole antennas.

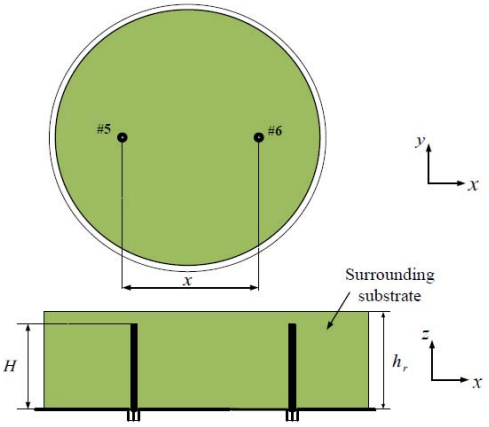

Fig. 7. Top and view of full dielectric coupled monopole antennas.

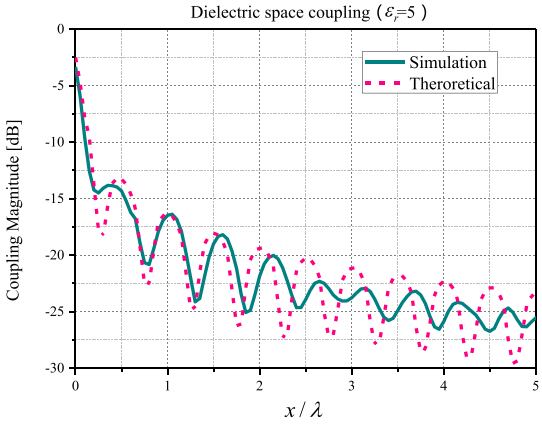

Fig. 8. Dielectric layer coupling comparison for the theoretical results and simulation results between monopole antennas.

constant in the three cases so that the same antenna design could be used, and would not have to be retuned for each substrate. The antennas are placed along the x-axis, as shown in Fig. 3(b). The space between the antennas varies from 0.5λ to 5λ. The simulation results for the mutual coupling versus distance are plotted in Fig. 4.

Note that the theoretical results match the numerical results much well with the least-squares technique once the gain parameters are determined, verifying the general form of (35). The slight difference between 0.5λ and 0.8λ is likely due to near-field effects, which are not included.

B. Monopole Antenna

As a second example, a monopole antenna surrounded by a thin dielectric substrate is shown in Fig. 5. The substrate has a thickness $h_r = 1.5$ mm, and relative dielectric constant ε_r of either 1 (the case of no substrate), 2.2, 4.4, or 10. The length of monopole is $H = 23.53$ mm, and it is fed by a coaxial line.

We evaluate the coupling between a pair of identical monopole antennas which are located on the infinite ground plane, the antennas are placed along the x-axis, as shown in Fig. 5. As with the patch antenna, we use a lossless surrounding substrate with the three different dielectric constants. For the three different surrounding substrates, the theoretical results and simulation results are in good agreement, as shown in Fig. 6. For the air substrate case, coupling is primarily due to free-space waves and the presence of oscillations is due to the small changes in phase between one or more surface waves and space waves for the relative dielectric constant ε_r of 10 case. Except for this, there is in good agreement between the calculated results and simulation results using (35) for various dielectric substrates.

Another example of the coupling between monopole antennas is shown in Fig. 7. All the parameters are the same as in Fig. 5, except that the substrate height h_r exceeds the height of the antennas. In this case, G3 is set to 0, the substrate has a relative dielectric constant ε_r of 5, and the length of monopoles has been tuned so that it is matched at 3 GHz. The purpose of this paper is to examine a case where surface-waves dominate. The simulated data from Fig. 8 shows sinusoidal variations that are likely due to interference between multiple surface modes which are present in the thick dielectric substrate. Based on the surface guided wave theory [28], we can obtain the cutoff frequencies as

$$f_c = \frac{n}{4h\sqrt{\varepsilon_d \mu_d - \varepsilon_0 \mu_0}} \quad n = 0, 2, 4 \ldots \tag{36}$$

From (36), we know there only two modes exist in this frequency range, so we may neglect higher order modes. Thus, neglecting differences in excitation strength between the

TABLE I
2-D AND 3-D GAIN VALUES FOR VARIOUS ANTENNAS AND VARIOUS DIELECTRIC SUBSTRATES

ε_r \ Type	Patch		Monopole		Slot		Monopole embedded	
	G_2	G_3	G_2	G_3	G_2	G_3	G_2	G_3
1	0.12	0.67	0.12	1.40	0.10	0.22	0.12	1.50
2.2	0.16	0.67	0.14	1.41	0.12	0.21	0.80	0.00
4.4	0.19	0.67	0.15	1.40	0.13	0.20	0.73	0.00
10	0.20	0.67	0.16	1.40	0.14	0.20	0.57	0.00

TABLE II
EFFECTIVE WIDTH AND EFFECTIVE APERTURE FOR VARIOUS ANTENNAS AND VARIOUS DIELECTRIC SUBSTRATES

ε_r \ Type	Patch		Monopole		Slot		Monopole embedded	
	W_{eff} (mm)	A_{eff} (cm^2)	W_{eff} (mm)	A_{eff} (cm^2)	W_{eff} (mm)	A_{eff} (cm^2)	W_{eff} (mm)	A_{eff} (cm^2)
1	1.9	5.3	1.9	11.1	1.6	1.7	1.9	11.9
2.2	2.5	5.3	2.2	11.2	1.9	1.7	12.7	0.0
4.4	3.0	5.3	2.4	11.1	2.1	1.6	11.6	0.0
10	3.2	5.3	2.5	11.1	2.2	1.6	9.1	0.0

two modes, (32) is changed to

$$\frac{P_r}{P_t} = G_{t2}G_{r2}\frac{\lambda}{4\pi^2 R}\cos[(k_{\mathrm{TM}_0} - k_{\mathrm{TM}_2})R] \tag{37}$$

where k_{TM0} and k_{TM2} correspond to the wavenumber of the first two surface-wave modes. There is a phase difference between the surface waves, so the simulation curve shows oscillations as a function of antenna separation. Because of neglecting the relative excitation strength of the two surface waves, the least-squares technique does not provide an exact match to the simulated data. Nonetheless, we can approximately fit (37) to the data.

IV. SUMMARY OF COUPLING COEFFICIENTS

We provide simulations of several simple examples and evaluate them in terms of 2-D gain G_2 and 3-D gain G_3, shown in Table I, as well as the effective width and effective aperture shown in Table II. For the first three examples, the operating frequency is 3 GHz ($\lambda = 100$ mm), the thickness of lossless surrounding substrate is 1.5 mm and dielectric constant is ε_r. In each case the antennas are well-matched ($S_{11} < -20$ dB). One case is the monopole embedded in a 20 mm thick dielectric, and retuned to match.

We also study the slot antenna, where the permittivity above the slot is kept fixed at 5 in order to avoid retuning the slot for each case, while the surrounding permittivity is varied. One way to reduce free-space coupling between antennas is to ensure that they do not have a direct line-of-sight path between them, such as by placing the antennas in cups or troughs. However, those features will also radiate, so free-space coupling cannot be entirely eliminated. The limiting case of a deep trough is simply a slot antenna, which is why it is included.

We can draw several conclusions from Tables I and II. First, the 3-D or space-wave gain of each antenna is roughly constant with substrate permittivity, as we expect. However, the 2-D or surface-wave gain increases with permittivity, which is also expected. The monopole has the highest G_3 toward the horizon, and the slot has the lowest. In terms of G_2, the patch has the highest value and the slot is the lowest. Thus, the patch and monopole are not ideal choices for minimizing coupling between antennas, and the slot appears to be the best choice regardless of the substrate. We know the least-squares technique only produces an estimate of the best fit. Thus, several possible answers for G_2 and G_3 could produce the same curves. So here an average sensitivity $\bar{\varphi}$ is introduced

$$\overline{\varphi} = \frac{\sum_1^N \varphi}{N} = \frac{\sum_1^N \Delta\mathrm{LSE}}{\Delta G_3 \cdot N} = \frac{\sum_1^N |D_{\mathrm{sim}} - D_{\mathrm{fitting}}|^2}{\Delta G_3 \cdot N} \tag{38}$$

where φ is the sensitivity for different points N in the distance of five wavelengths between antennas, Δ LSE is the least-square error, ΔG_3 is the difference of changed G_3, D_{sim}, and D_{fitting} are simulation data and fitting curve data, respectively. For embedded antennas (EA), the $\overline{\varphi}_{\mathrm{EA}} = 0$ can be obtained from (38) when the G_3 value varies from 0 to 2. Thus, the curve fitting has a high degree of uncertainty for G_3 and a unique solution for G_2 in this case. In other words, surface waves become much more significant whereas free space waves can be ignored. Compared with the EA case, we get an average sensitivity of $\overline{\varphi}_P = 20$ for the patch case when the G_3 value is changed from 0.60 to 0.72. So the curve fitting has a unique solution for both G_2 and G_3. Similarly, monopole antenna has an average sensitivity of $\overline{\varphi}_m = 5.7$ when the G_3 value varies from 1.43 to 1.56. Thus, the curve fitting has a unique solution for both G_2 and G_3. In the case of slot antennas, the average sensitivity is $\overline{\varphi}_s = 5.6$ when the G_3 value is changed from 0.16 to 0.25. Hence, the curve fitting also has a unique solution for both G_2 and G_3.

Note that the gain of the monopole is 1.5 rather than 3. As we know, the transmission between two dipoles in free space is the same as the transmission between two equivalent monopoles sharing the same ground plane, because the ground plane simply acts as a symmetry plane in an otherwise identical problem. Logan and Rockway [29] and Trainotti *et al.* [30] have explained this by showing that antennas on a ground plane have different values for transmit gain and receive gain, e.g., $G_t = 3$ and $G_r = 0.75$ for transmitting and receiving monopoles. Because we are interested in mutual coupling in both directions, we avoid any confusion in this regard by simply using the geometric mean of the transmitting and receiving gain values

$$G_3 = \sqrt{G_{t3}G_{r3}} \quad G_2 = \sqrt{G_{t2}G_{r2}}. \tag{39}$$

Our final transmission equation is as follows:

$$\frac{P_r}{P_t} = G_3^2\left(\frac{\lambda}{4\pi R}\right)^2 + G_2^2\frac{\lambda}{4\pi^2 R} + 2G_3G_2\frac{\lambda}{4\pi R}\sqrt{\frac{\lambda}{4\pi^2 R}}. \tag{40}$$

V. RELATIVE CONTRIBUTION OF SURFACE WAVES

A plot of the total mutual coupling between a pair of conventional rectangular microstrip patch antennas, a pair of

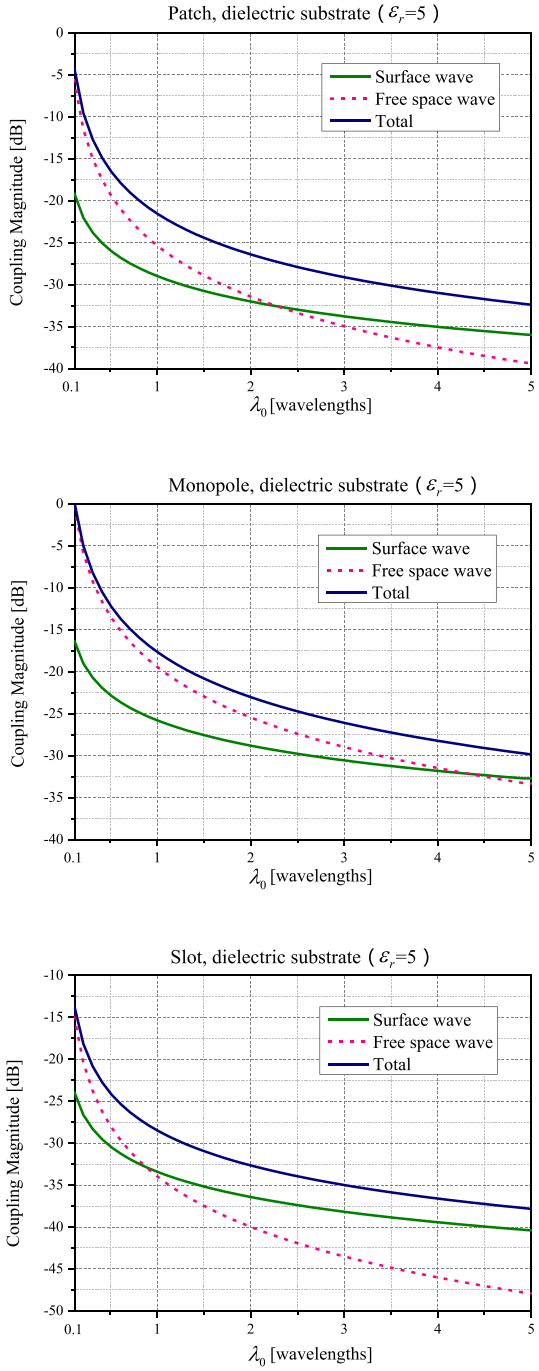

Fig. 9. Different components of the mutual coupling between different types of antennas.

monopole antennas, and a pair of slot antennas is shown in Fig. 9. Considering that the thickness of the slab is very small, the wavenumber k_{TM} is almost equal to the wavenumber k_0 [25], so the $\cos\theta_R$ term is negligible. After fitting to determine G_2 and G_3, the free-space and surface-wave contributions can be plotted separately. The navy curve is total coupling from simulated data between antennas, and it is divided into free-space coupling (pink) and surface-wave coupling (dark cyan). This plot closely matches previous analytical studies of the microstrip antenna coupling [1].

From Fig. 9, we can see that there is a crossing point between surface-wave coupling and free-space wave coupling.

TABLE III

FREE-SPACE WAVE/SURFACE-WAVE CROSSING POINT FOR VARIOUS SUBSTRATE DIELECTRIC CONSTANTS AND ANTENNA TYPES

ε_r \ Type	Patch	Monopole	Slot
	Crossing Point	Crossing Point	Crossing Point
1	-37.1 dB	-37.2 dB	-37.0 dB
2.2	-34.0 dB	-34.1 dB	-34.0 dB
4.4	-32.5 dB	-32.4 dB	-32.4 dB
10	-29.5 dB	-29.5 dB	-28.4 dB

Referring to formula (40), the distance of crossing point can be given by

$$G_3^2\left(\frac{\lambda}{4\pi R'}\right)^2 = G_2^2\frac{\lambda}{4\pi^2 R'}. \tag{41}$$

Because the two antennas are identical, the formula can be rewritten to determine the distance beyond which the surface-wave coupling dominates

$$R' = \frac{\lambda}{4}\left(\frac{G_3}{G_2}\right)^2 = \frac{1}{\lambda}\left(\frac{A_{\mathrm{eff}}}{W_{\mathrm{eff}}}\right)^2. \tag{42}$$

Free-space wave coupling is dominant for $R < R'$, and surface-wave coupling is dominant for $R > R'$. For this patch example, R' is approximately 2.5λ, as shown in Fig. 9. For the case of the monopole and the slot, R' is approximately 4.3λ and 0.8λ, respectively. At much shorter distances, (closer than $\lambda/2\pi$) coupling is dominated by the near fields.

Based on this analysis, the control of mutual coupling can be explained by the following steps in order of importance. Some of these may not be possible depending on the application.

1) Keep the separation distance much greater than the boundary of the near-field region ($R \gg \lambda/2\pi$).
2) Arrange the antennas such that they each have a null in their pattern toward the other antenna if possible.
3) Minimize free-space coupling by ensuring that the antennas do not have line-of-sight exposure to each other (i.e., slots are preferred over monopoles).
4) Minimize surface-wave coupling by choice of substrate or by other means (e.g., reactive surfaces).

Note that although control of the surface-wave coupling is often the focus of research, it is the last issue that should be addressed after dealing with the near-field and free-space coupling because it only dominates at greater distances. Based on the analysis above, the relevant distance where they become important is on the order of a few wavelengths, depending on antenna and substrate type. Nonetheless, in applications where coupling requirements are extremely low, i.e., less than -30 dB, control of surface waves becomes important.

Note that in Fig. 9, although each antenna type had a different value of R', the magnitude of the coupling at R' was the same for all antenna types. In Table III, we compare the magnitude of coupling at R' for various substrates and antenna types. We find that the magnitude of the crossing point is independent of the antenna type, and only depends on the substrate. Thus, for a given substrate, it is possible to determine the coupling magnitude below which surface waves

must be controlled. For example, on a bare ground plane with no dielectric, if coupling of higher than -37 dB, then surface waves are not significant.

VI. Conclusion

In this paper, we introduce the effective width of an antenna with respect to surface-wave radiation and derive the effective width of an isotropic surface-wave radiator. We determine the directivity of a surface-wave radiator for various radiation modes, including a planar dipole pattern and a vertical monopole pattern. We then add the 2-D surface-wave propagation component to the Friis transmission equation. By the comparison of the theoretical results and the numerical results on mutual coupling between pairs of antennas, the relative contributions of surface waves and free-space waves can be separated.

We also defined the distance beyond which surface waves dominate in terms of the 2-D and 3-D gain components, and found that this distance is on the order of a few wavelengths, depending on the antenna type. For the design that is most effective at minimizing free-space coupling (the slot antenna), the surface waves are the most important coupling mechanism, and they dominate the coupling at distances beyond one wavelength.

The ultimate purpose of this paper is for antenna designers to understand the relative contributions of surface waves, free-space waves, and antenna design considerations to the mutual coupling. At distances of a few wavelengths, coupling can be controlled primarily by using low-profile antenna elements, and if possible by controlling their orientation to minimize gain along the horizon. Only after these issues have been addressed should the designer be concerned with surface waves. Finally, we provide a way to quantify surface-wave coupling in terms of the 2-D gain G_2.

References

[1] M. A. Khayat, J. T. Williams, D. R. Jackson, and S. A. Long, "Mutual coupling between reduced surface-wave microstrip antennas," *IEEE Trans. Antennas Propag.*, vol. 48, no. 10, pp. 1581–1593, Oct. 2000.

[2] E. M. Koper, W. D. Wood, and S. W. Schneider, "Aircraft antenna coupling minimization using genetic algorithms and approximations," *IEEE Trans. Aerosp. Electron. Syst.*, vol. 40, no. 2, pp. 742–751, Apr. 2004.

[3] D. A. Tsyanenka, E. V. Sinkevich, and A. A. Matsveyeu, "Computationally-effective worst-case model of coupling between on-board antennas that takes into account diffraction by conducting hull," in *Proc. IEEE Int. Symp. Electromagn. Compat. (EMC EUROPE)*, Sep. 2016, pp. 602–607.

[4] P. N. Fletcher, M. Dean, and A. R. Nix, "Mutual coupling in multi-element array antennas and its influence on MIMO channel capacity," *Electron. Lett.*, vol. 39, no. 4, pp. 342–344, Feb. 2003.

[5] B. N. Getu and R. Janaswamy, "The effect of mutual coupling on the capacity of the MIMO cube," *IEEE Antennas Wireless Propag. Lett.*, vol. 4, pp. 240–244, 2005.

[6] I. J. Gupta and A. Ksienski, "Effect of mutual coupling on the performance of adaptive arrays," *IEEE Trans. Antennas Propag.*, vol. AP-31, no. 5, pp. 785–791, Sep. 1983.

[7] E. M. Friel and K. M. Pasala, "Effects of mutual coupling on the performance of STAP antenna arrays," *IEEE Trans. Aerosp. Electron. Syst.*, vol. 36, no. 2, pp. 518–527, Apr. 2000.

[8] J.-W. Yook and L. P. B. Katehi, "Micromachined microstrip patch antenna with controlled mutual coupling and surface waves," *IEEE Trans. Antennas Propag.*, vol. 49, no. 9, pp. 1282–1289, Sep. 2001.

[9] M. M. Nikolic, A. R. Djordjevic, and A. Nehorai, "Microstrip antennas with suppressed radiation in horizontal directions and reduced coupling," *IEEE Trans. Antennas Propag.*, vol. 53, no. 11, pp. 3469–3476, Nov. 2005.

[10] R. E. Collin, *Foundations for Microwave Engineering*. NewYork, NY, USA: McGraw-Hill, 1992.

[11] M. Salehi, A. Motevasselian, A. Tavakoli, and T. Heidari, "Mutual coupling reduction of microstrip antennas using defected ground structure," in *Proc. 10th IEEE Int. Conf. Commun. Syst.*, Oct./Nov. 2006, pp. 1–5.

[12] Y. Hajilou, H. R. Hassani, and B. Rahmati, "Mutual coupling reduction between microstrip patch antennas," in *Proc. 6th EUCAP*, Mar. 2012, pp. 1–4.

[13] J. Ouyang, F. Yang, and Z. M. Wang, "Reducing mutual coupling of closely spaced microstrip MIMO antennas for WLAN application," *IEEE Antennas Wireless Propag. Lett.*, vol. 10, pp. 310–313, 2011.

[14] A. Habashi, J. Nourinia, and C. Ghobadi, "Mutual coupling reduction between very closely spaced patch antennas using low-profile folded split-ring resonators (FSRRs)," *IEEE Antennas Wireless Propag. Lett.*, vol. 10, pp. 862–865, 2011.

[15] F. Yang and Y. Rahmat-Samii, "Microstrip antennas integrated with electromagnetic band-gap (EBG) structures: A low mutual coupling design for array applications," *IEEE Trans. Antennas Propag.*, vol. 51, no. 10, pp. 2936–2946, Oct. 2003.

[16] M. Niroo-Jazi, T. A. Denidni, M. R. Chaharmir, and A. R. Sebak, "A hybrid isolator to reduce electromagnetic interactions between Tx/Rx antennas," *IEEE Antennas Wireless Propag. Lett.*, vol. 13, pp. 75–78, 2014.

[17] H. S. Farahani, M. Veysi, M. Kamyab, and A. Tadjalli, "Mutual coupling reduction in patch antenna arrays using a UC-EBG superstrate," *IEEE Antennas Wireless Propag. Lett.*, vol. 9, pp. 57–59, 2010.

[18] D. Sievenpiper, L. Zhang, R. F. J. Broas, N. G. Alexopolous, and E. Yablonovitch, "High-impedance electromagnetic surfaces with a forbidden frequency band," *IEEE Trans. Microw. Theory Techn.*, vol. 47, no. 11, pp. 2059–2074, Nov. 1999.

[19] A. C. Durgun, C. A. Balanis, C. R. Birtcher, H. Huang, and H. Yu, "High-impedance surfaces with periodically perforated ground planes," *IEEE Trans. Antennas Propag.*, vol. 62, no. 9, pp. 4510–4517, Sep. 2014.

[20] E. Rajo-Iglesias, Q. Uevedo-Teruel, and L. Inclan-Sanchez, "Planar soft surfaces and their application to mutual coupling reduction," *IEEE Trans. Antennas Propag.*, vol. 57, no. 12, pp. 3852–3859, Dec. 2009.

[21] Ó. Quevedo-Teruel, L. Inclan-Sanchez and E. Rajo-Iglesias, "Soft surfaces for reducing mutual coupling between loaded PIFA antennas," *IEEE Antennas Wireless Propag. Lett.*, vol. 9, pp. 91–94, 2010.

[22] *National Radio Astronomy Observatory*. Univ. Virginia, Blackbody Radiation. Accessed on Sep. 2008. [Online]. Available: http://www.cv.nrao.edu/course/astr534/BlackBodyRad.htmls

[23] J. H. Jeans, "XI. On the partition of energy between matter and aether," *Philos. Mag.*, vol. 10, pp. 91–98, no. 55, 1905.

[24] J. W. S. Rayleigh, "The dynamical theory of gases and of radiation," *Nature*, vol. 72, no. 1855, pp. 54–55, 1905.

[25] J. Jian-Ming, *Theory and Computation of Electromagnetic Fields*. New York, NY, USA: Wiley, 2011.

[26] J. R. Wait, "The ancient and modern history of EM ground-wave propagation," *IEEE Antennas Propag. Mag.*, vol. 40, no. 5, pp. 7–24, Oct. 1998.

[27] N. Chahat, G. Valerio, M. Zhadobov, and R. Sauleau, "On-body propagation at 60 GHz," *IEEE Trans. Antennas Propag.*, vol. 61, no. 4, pp. 1876–1888, Apr. 2013.

[28] R. F. Harrington, *Time—Harmonic Electromagnetic Fields*. New York, NY, USA: Wiley, 2001.

[29] J. C. Logan and J. W. Rockway, "Dipole and monopole antenna gain and effective area for communication formulas," Naval Command, Control Ocean Surveill. Center, RDT&E Division, San Diego, CA, USA, Tech. Rep. 1756, Sep. 1997.

[30] V. Trainotti and G. Figueroa, "Vertically polarized dipoles and monopoles, directivity, effective height and antenna factor," *IEEE Trans. Broadcast.*, vol. 56, no. 3, pp. 379–409, Sep. 2010.

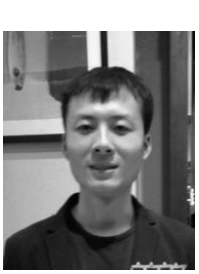

Chao Wang (S'14) received the B.Sc. degree in electrical engineering from the Xi'an University of Posts and Telecommunications, Xi'an, China, in 2010, and the Ph.D. degree in electromagnetic fields and microwave technology from the University of Electronic Science and Technology of China, Chengdu, China, in 2017.

He was a Visiting Graduate Student with the Applied Electromagnetics Research Group, University of California at San Diego, La Jolla, CA, USA, from 2015 to 2017. His current research interests include ultrawideband antenna, theoretical arithmetic for surface-wave attenuation, and impedance surfaces for reducing mutual coupling between antennas.

En Li (M'14) received the M.S. degree in physical electronics and the Ph.D. degree in electromagnetic field and microwave technology from the University of Electronic Science and Technology of China, Chengdu, China, in 2003 and 2009, respectively.

He is currently a Professor with the University of Electronic Science and Technology of China. He has authored or co-authored over 100 journal, conference papers, and 12 authorized national invention patents.

His current research interests include microwave plasma diagnosis, electromagnetic parameter measurement of dielectric material at high temperatures, nonlinear parameter measurement of high-power amplifier, and design of microwave devices.

Dr. Li was a receipient of the Second Prize of The National Science and Technology Progress Award, the First Prize, the Second Prize, and the Third Prize of the Provincial And Ministerial Level Scientific and Technological Progress Awards. In 2010, he was a winner of Education Ministry's New Century Excellent Talents Supporting Plan, a receipient of the title of excellent experts with outstanding contribution of Sichuan Province in 2013. He is a Guest Professor with the National Defense Science and Technology Key Laboratory of Advanced Function Composite Material.

Daniel F. Sievenpiper (M'94–SM'04–F'09) received the B.S. and Ph.D. degrees in electrical engineering from the University of California, Los Angeles, CA, USA, in 1994 and 1999, respectively.

He was the Director with the Applied Electromagnetics Laboratory, HRL Laboratories, Malibu, CA, USA, where he was invoved in artificial impedance surfaces, conformal antennas, tunable and wearable antennas, and beam steering methods. He is currently a Professor with the University of California, San Diego, CA, USA, where he is focused on antennas and electromagnetic structures. He has more than 70 issued patents and more than 120 technical publications.

Dr. Sievenpiper was awarded the URSI Issac Koga Gold Medal in 2008. Since 2010, he has been served as an Associate Editor of the IEEE ANTENNAS AND WIRELESS PROPAGATION LETTERS.